

## Trapping time of excitons in Si nanocrystals embedded in a SiO<sub>2</sub> matrix

E. M. L. D. de Jong,<sup>1,\*</sup> W. D. A. M. de Boer,<sup>1,2</sup> I. N. Yassievich,<sup>3</sup> and T. Gregorkiewicz<sup>1</sup>

<sup>1</sup>*Van der Waals-Zeeman Institute, University of Amsterdam, Science Park 904, 1098 XH Amsterdam, The Netherlands*

<sup>2</sup>*Department of Biological Sciences, Columbia University, 906 NWC Building, 550 West 120 Street, New York, New York 10027, USA*

<sup>3</sup>*Ioffe Physical-Technical Institute, Russian Academy of Sciences Polytechnicheskaya 26, 194021 Saint-Petersburg, Russia*

(Received 14 February 2017; revised manuscript received 18 April 2017; published 22 May 2017)

Silicon (Si) nanocrystals (NCs) are of great interest for many applications, ranging from photovoltaics to optoelectronics. The photoluminescence quantum yield of Si NCs dispersed in SiO<sub>2</sub> is limited, suggesting the existence of very efficient processes of nonradiative recombination, among which the formation of a self-trapped exciton state on the surface of the NC. In order to improve the external quantum efficiency of these systems, the carrier relaxation and recombination need to be understood more thoroughly. For that purpose, we perform transient-induced absorption spectroscopy on Si NCs embedded in a SiO<sub>2</sub> matrix over a broad probe range for NCs of average sizes from 2.5 to 5.5 nm. The self-trapping of free excitons on surface-related states is experimentally and theoretically discussed and found to be dependent on the NC size. These results offer more insight into the self-trapped exciton state and are important to increase the optical performance of Si NCs.

DOI: [10.1103/PhysRevB.95.195312](https://doi.org/10.1103/PhysRevB.95.195312)

### I. INTRODUCTION

The semiconductor silicon (Si) is investigated thoroughly because of its interesting fundamental properties and its large abundance. It is applied broadly in optoelectronics [1,2], photonics [3], photovoltaics [4–6], and medicine [7], among others. Besides bulk and porous Si, nanocrystals (NCs) also have attracted much attention due to quantum confinement resulting in size-tunable photoluminescence (PL), discrete structure of the energy states, and relaxing the momentum conservation described by Heisenberg's uncertainty principle. The PL properties of Si NCs have been investigated widely in experiment as well as theory, showing that the band gap opens and the radiative rate increases with decreasing NC size [8]. Stabilization of the PL emission energy for oxygen-terminated Si NCs smaller than  $\sim 2.5$  nm in diameter has been observed [9], which is not predicted by the size quantization. It has been suggested that it originates from oxygen-related defects at the surface of the NCs, which introduce levels in the band gap and participate in carrier recombination [9]. The formation of a self-trapped exciton (STE) state has been proposed among other possibilities [10]. Direct experimental evidence confirming the formation of the STE state was given only recently from studies of the free-carrier dynamics of Si NCs embedded in a SiO<sub>2</sub> matrix [11,12]. When probed at high energies, the induced absorption (IA) signal of this material features a long-living component for high probe energies, whereas it vanishes within less than a nanosecond for lower probe energies; this has been explained by self-trapping of excitons on surface-related states [11,12]. Although a possible return of carriers from the STE state to the free exciton (FE) state was discussed [13], details on the trapping process are, however, presented here. Building on previous results, we now investigate the trapping process of free carriers into the STE state by means of a conventional pump-probe setup. The

trapping behavior is of great importance to obtain a complete understanding of the details of the mechanisms responsible for the light emission in Si NCs and for their application potential.

### II. EXPERIMENTAL DETAILS

The studied samples feature closely packed Si NCs embedded in a SiO<sub>2</sub> matrix and are prepared by a radio-frequency cosputtering method. The deposited films are annealed in a nitrogen gas atmosphere for 30 min at temperatures ranging from 1000 to 1200 °C. By tuning this annealing temperature and the excess of Si in the sputtering process, samples with average NC sizes  $d_{\text{NC}}$  ranging from 2.5 to 5.5 nm ( $\sigma \sim 19\%$ ) are fabricated [14].

A pump-probe setup is used to investigate the IA dynamics for different probe energies. The fundamental output beam ( $E_{\text{fund}} = 1.55$  eV) of a Ti:sapphire laser with a repetition rate of  $f = 1$  kHz (Spectra-Physics) is split into two parts. The first path is directly onto an optical parametric amplifier to generate an excitation pump energy of  $E_{\text{exc}} = 3.6$  eV. The second path is converted to a broadband white-light continuum ( $E_{\text{probe}} = 1.6\text{--}3.25$  eV) with the aid of a calcium fluoride plate in order to enable energy-resolved probing. The probe pulse is delayed with respect to the pump pulse by means of a (folded) optical delay stage, allowing for a time window of several nanoseconds. The IA signal is detected with a multichannel charge-coupled device camera (Ocean Optics) such that the entire spectral range of the probe pulse can be registered for each time delay between the pump and the probe pulse. The IA signal  $I_{IA}$  is determined as

$$I_{IA} = \log_{10} \left( \frac{I_{T,\text{off}}}{I_{T,\text{on}}} \right), \quad (1)$$

where  $I_{T,\text{off}}$  and  $I_{T,\text{on}}$  are the transmitted probe fluence with the pump laser off and on, respectively. All optical measurements are performed at room temperature in ambient air.

\*E.M.L.D.deJong@uva.nl

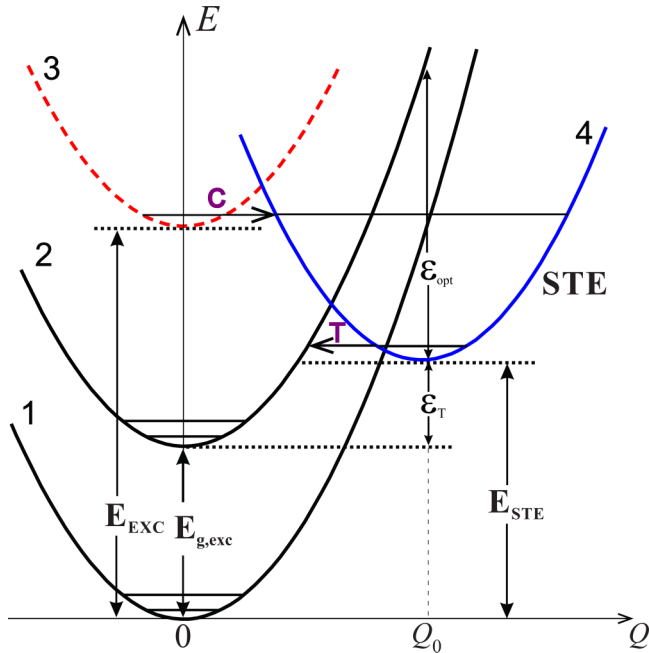


FIG. 1. Schematic of the adiabatic vibrational potentials, including the STE state, in the framework of the Huang-Rhys model within a configuration coordinate diagram. Potential 1 corresponds to the system before an excitation is created, and adiabatic potentials 2 and 3 correspond to the ground ( $E_{g,\text{exc}}$ ) and excited ( $E_{\text{EXC}}$ ) exciton states in the NC, respectively. Potential 4 represents the STE with energy  $E_{\text{STE}}$ ,  $\varepsilon_{\text{opt}}$  is the threshold energy of optical ionization from the STE state, and  $\varepsilon_T$  is the energy of the thermal ionization of an electron from the ground exciton state to the STE state. Arrow  $C$  shows the process of the exciton capture from the excited state to the STE state, and  $T$  demonstrates the process of the thermally stimulated tunneling from the ground state in potential 4 to potential 2.

### III. PRELIMINARIES: SELF-TRAPPED EXCITON STATE IN SI NANOCRYSTALS

The free-carrier dynamics of Si NCs feature a multiexponential decay indicating several relaxation pathways, among which trapping [15] and radiative recombination. After photoexcitation with a pump energy of  $E_{\text{exc}} = 3.6$  eV, the excited electron-hole pairs mainly consist of hot electrons and cold holes; in this paper, we assume that situation basing ourselves on calculations presented in Ref. [16]. The nonequivalent energy distribution between holes and electrons may be explained as originating from the  $\Gamma$  and  $X$  valleys mixing, which takes place for the hot electrons localized in the Si NCs, shifting the maximum of the electron-density distribution in  $k$  space from  $k_0 = (2\pi \cdot 0.85)/a$  (where  $a$  is the bulk lattice constant) towards the  $\Gamma$  point considerably (see Ref. [17]). Besides cooling down to the bottom of the band edges, the hot carriers can also be captured into the self-localized state, associated with the Si-O bond at the surface, thereby reducing the free-carrier concentration [11,12]. The trapping of the electron and holes leads to the formation of a STE. This STE scenario can be described within the framework of the Huang-Rhys model with a configuration coordinate diagram, which is schematically presented in Fig. 1. The energy  $E$  in Fig. 1 corresponds to the sum of the energy of an exciton and

the local vibration energy of the surface defect, associated with the Si-O bond. The adiabatic potential of the NC without an exciton is represented by parabola 1 ( $E_0 = \hbar\omega_0/2$ , where  $\hbar\omega_0$  is the energy of the local vibration phonon). Parabolic potential curves 2–4 correspond here to an exciton in the ground state, excited state, and trapped at the STE state, respectively. Due to the interaction between the STE and the local vibration mode, the parabola representing the STE is horizontally shifted to the configuration coordinate  $Q_0$ . The energy position of the ground STE state is independent of the NC size [9,11,12], but the ground FE state (parabola 2) shifts up in energy when the NC size is reduced, corresponding to the opening of the NC band gap due to quantum confinement. The energy position of the ground STE state  $E_{\text{STE}}$  is taken equal to the energy of the ground FE state of a Si NC with a 2.5-nm diameter:  $E_{\text{STE}} \simeq E_{g,\text{exc},2.5\text{ nm}}$ , following Refs. [9,11]. It takes into account that no blueshift of the PL is observed for NC sizes below  $d_{\text{NC}} \lesssim 2.5$  nm [9]. When the NC size is smaller than 2.5 nm, the STE forms the energy level in the energy gap. The value of  $\varepsilon_T$  in Fig. 1 is determined by the difference between the ground STE and the ground FE state of the NC under consideration:  $\varepsilon_T = E_{\text{STE}} - E_{g,\text{exc}}$ . It goes to zero for a NC size of 2.5 nm.

When a free hot exciton is captured from the NC into the STE state to a high vibrational level (process indicated with  $C$  in Fig. 1), it can relax to the ground STE state by the emission of local phonons. Once captured in the ground STE state, the excitons also can return to the FE state by thermally activated tunneling (process indicated with  $T$  in Fig. 1) or by the absorption of a (probe) photon with an energy larger than a certain threshold  $\varepsilon_{\text{opt}}$  (see Fig. 1), which depends on the NC size (see Refs. [11,12] for more details). The trapping of hot free excitons with energy  $E$  is accompanied by multiphonon transitions. It is efficient and usually occurs within a few picoseconds, whereas the reversed thermally activated tunneling time from the ground STE state into the FE state is much longer for the investigated NC sizes [11,12].

The Huang-Rhys factor  $S_{HR}$ , which determines the probability of multiphonon transitions, in the case of a metastable STE state ( $E_{\text{STE}} > E_{g,\text{exc}}$ ) is given by

$$S_{HR} = \frac{\varepsilon_{\text{opt}} + \varepsilon_T}{\hbar\omega_0}. \quad (2)$$

For the 2.5-nm-sized NCs ( $\varepsilon_T \simeq 0$  eV), a value of  $\varepsilon_{\text{opt}} \simeq 2.75$  eV was previously experimentally determined [11]. Equation (2) results in a Huang-Rhys factor of  $S_{HR} \simeq 20$  for the phonon energy of the Si-O vibrational mode  $\hbar\omega_0 = 140$  meV. This large value shows that the electron-phonon coupling is very strong. Similar strong electron-phonon coupling has been observed and theoretically discussed before for dangling bond-related levels [18,19].

The displacement of the bottom of the adiabatic potential corresponding to the STE state  $Q_0$  (see Fig. 1) is given by the relation,

$$\frac{M\omega_0^2 Q_0^2}{2} = \varepsilon_{\text{opt}} + \varepsilon_T, \quad (3)$$

where  $M$  is the mass of the vibrating particle. It is convenient to introduce the dimensionless coordinate,

$$x_0 = \sqrt{\frac{M\omega_0}{\hbar}} Q_0 = \sqrt{2S_{HR}}, \quad (4)$$

resulting in  $x_0 = 6.36$ , independent of the NC size.

#### IV. EXPERIMENTAL RESULTS

In Fig. 2, a typical IA dynamics, in the inset a zoom into the first 30 ps, is shown for the sample with an average NC diameter of  $d_{NC} = 5.5$  nm under 3.6-eV excitation for two different probe energies of 1.8 and 3.0 eV, below and above the STE threshold energy for optical excitation from the STE to the FE state  $\varepsilon_{opt}$  (see Fig. 1) [11]. The 1.8-eV IA transient decays practically to zero within the time window of 3 ns, whereas the trace representing the higher probe energy of 3.0 eV features a longer-living component. Previously [11,12], this behavior has been assigned to the self-trapping of excitons on surface-related states where the trapped carriers can be released into the FE state after absorption of a high-energy photon ( $E_{probe} > \varepsilon_{opt}$ ). In order to investigate the initial fast decay of the IA signal in the first picoseconds in more detail, the measurements also are performed on samples with different average NC sizes. The results for a probe energy of 1.8 eV ( $E_{probe} < \varepsilon_{opt}$  for all investigated  $d_{NC}$ 's) are shown in Fig. 3, indicating that the decay accelerates with decreasing NC size. Thus, the results suggest that the initial fast decay in the first picoseconds is dependent on the NC size as well as probe energy. We note that a possible presence of multiexcitons undergoing Auger recombination will not lead to the observed  $E_{probe}$ -dependent initial fast decay.

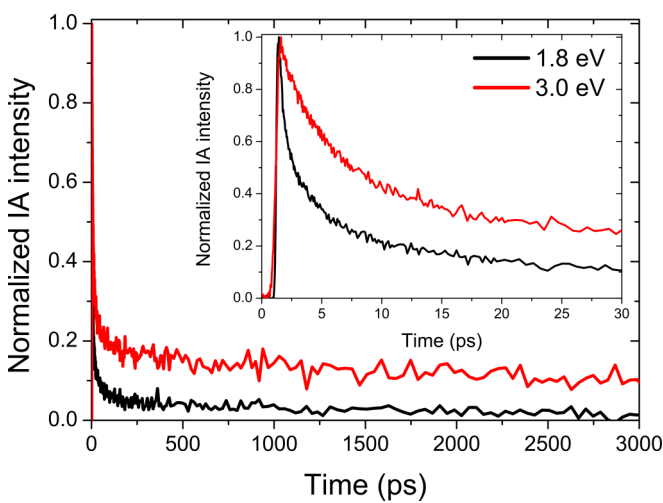


FIG. 2. Probe energy dependence of the IA transients. Normalized IA intensity transients for the sample with an average NC diameter of  $d_{NC} = 5.5$  nm with the probe energy set to below ( $E_{probe} = 1.8$  eV, black curve) and above ( $E_{probe} = 3.0$  eV, red curve) the STE ionization threshold energy of this sample. In the inset, a zoom into the first 30 ps is shown.

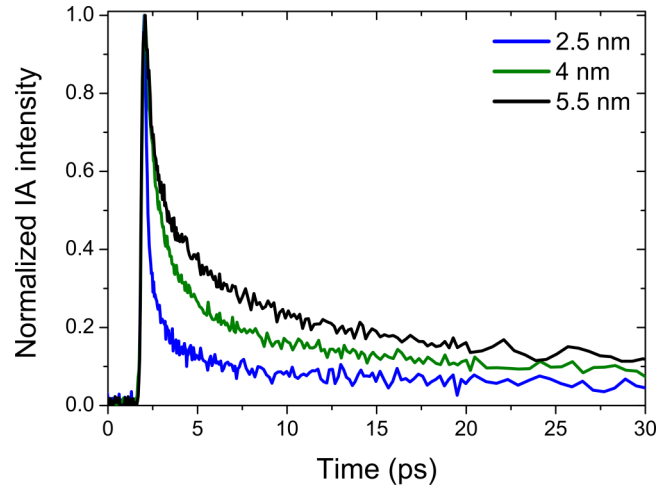


FIG. 3. Influence of the NC size on the IA transients. Normalized IA intensity transients for a probe energy of  $E_{probe} = 1.8$  eV for samples with different average NC sizes  $d_{NC}$  of 2.5 (blue), 4 (olive), and 5.5 nm (black).

#### V. THEORETICAL MODEL

Building on the STE model as described in Sec. III, we will now discuss the capture of a hot exciton, formed upon photon absorption, from the Si NC core states to the self-localized state related to the surface trap due to the Si-O bond. The probability of the exciton capture into the STE state on the Si NC surface  $W_{exc}$  is given by the expression,

$$W_{exc} = \frac{2\pi}{\hbar} \sum_{n'} |t_{exc}|^2 |\langle \Phi_{n'} | \Phi_0 \rangle|^2 \delta(E_i - E_f), \quad (5)$$

where the initial energy of the system under consideration  $E_i$  (the sum of the optically excited hot-exciton energy and the surface-trap vibration mode at the ground level with energy  $\hbar\omega_0/2$ ) is  $E_i = E_e + E_h + E_g + \hbar\omega_0/2$ , the final energy is  $E_f = E_{STE} + (n' + 1/2)\hbar\omega_0$ ,  $|t_{exc}|$  is the matrix element controlling the exciton tunneling, and  $|\langle \Phi_{n'} | \Phi_0 \rangle|$  is the overlap integral of the vibration functions in the initial and final states with energies  $(\hbar\omega_0/2)$  and  $(n' + 1/2)\hbar\omega_0$ , respectively.

We suppose that the exciton capture into the STE state is determined by the electron tunneling into the surface-trap state, whereas the hole is staying in the space-quantized NC ground state. The initial electron energy  $E_e$  is smoothed on the value  $\delta E$ :  $E_e \Rightarrow E_e + \delta E$ , and Eq. (5) is averaged over the energy interval  $(\hbar\omega_0)$ , taking into account the discrete character of the vibration energy. In result, Eq. (5) will be simplified to

$$W_{exc} = \frac{2\pi}{\hbar^2\omega_0} |t_e|^2 |\langle \Phi_n | \Phi_0 \rangle|^2, \quad (6)$$

where  $t_e$  is the matrix element of electron tunneling. The process of electron tunneling is accompanied by the transformation of the hot-electron energy in the excitation of the trap vibration mode at level  $n$ . It is convenient to rewrite Eq. (6) in the form

$$W_{exc} = w_e |\langle \Phi_n | \Phi_0 \rangle|^2, \quad (7)$$

where

$$w_e = \frac{2\pi}{\hbar^2 \omega_0} |t_e|^2 \quad (8)$$

determines the probability of the electron tunneling.

Matrix element  $t_e$  can be calculated using the simplified model for Si NCs assuming a spherical NC with an infinitely high barrier and the isotropic effective mass for electrons  $m^* \simeq 0.33m_0$ . In this approximation, the space-quantized energy levels are given by

$$E_{nl} = \frac{\hbar^2}{2m^* R^2} \varphi_{nl}^2, \quad (9)$$

where  $R$  is radius of the NC,  $\varphi_{nl}$  is the  $n$ th root of the spherical Bessel function  $j_l(x)$ :  $j_l(\varphi_{nl}) = 0$ , and the normalized wave functions of the electrons are given by

$$\psi_e = \psi_{nlm}(\vec{r}) = \sqrt{\frac{2}{R^3}} Y_{lm}(\theta, \phi) \frac{j_l(\varphi_{nl} r/R)}{j_{l+1}(\varphi_{nl})}, \quad (10)$$

where  $Y_{lm}(\theta, \phi)$  are the normalized spherical harmonics.

The approach of the zero-radius potential model [20] can be used to describe the wave function of the electron localized into the surface trap,

$$\psi_t = \sqrt{\frac{\kappa}{2\pi}} \frac{e^{-\kappa|\vec{r}-\vec{r}_t|}}{|\vec{r}-\vec{r}_t|}, \quad (11)$$

with

$$\kappa = \frac{\sqrt{2mE_t}}{\hbar}. \quad (12)$$

$\vec{r}_t$  is here the trap position on the Si NC surface, and  $E_t$  is the energy calculated from the boundary of the continuous energy spectrum (the bottom of the conduction band of SiO<sub>2</sub>), hereinafter referred to as the tunneling energy, and is given by the relation,

$$E_t = U_e - E_e, \quad (13)$$

where the height of the NC potential barrier  $U_e$  (which is 3.2 eV [21,22]) and the electron energy  $E_e$  are both calculated from the bottom of the conduction band of bulk Si. In our approach, the matrix element of the electron tunneling into the STE state  $t_e$  depends on the height of the barrier for tunneling  $E_t$ , which is given by Eq. (13) and the overlap of the electron wave functions in the initial state in the NC  $\psi_e$  and in the final state in the trap  $\psi_t$ . As a result,  $t_e$  is given by

$$t_e = E_t |\langle \psi_t | \psi_e \rangle|. \quad (14)$$

We remark that Eq. (14) takes into account that the electron wave functions exist only inside the NC, hence  $t_e$  is determined only by the ‘‘tail’’ of the trap wave function. Consequently, the electron probability of tunneling  $w_e$ , with taking into account Eq. (10), can be presented in the form

$$w_e = \frac{2\pi E_t^2}{\hbar^2 \omega_0} \frac{1}{(2l+1)} \sum_m |\langle \psi_t | \psi_{nlm} \rangle|^2. \quad (15)$$

Here, we have taken into account that there are  $2l+1$  levels with the same energy  $E_{nl}$  for  $m = -l, -l+1, \dots, l-1, l$ .

## VI. COMPARISON OF EXPERIMENTAL AND THEORETICAL RESULTS

From the just discussed theoretical model, the probability of electron tunneling into the STE state  $w_e$  can be estimated and discussed in view of the experimental results. The NCs in this paper are excited with an excitation energy of  $E_{\text{exc}} = 3.6$  eV such that the electron and tunneling energies have values of  $E_e \simeq 2.3$  and  $E_t \simeq 1$  eV, respectively (depending on the NC size). Therefore the distance  $1/\kappa$  is very small compared to the NC radius  $R$  for all the investigated Si NCs [see Eq. (12)], and the matrix element  $t_e$  is determined only in the vicinity of the trap position  $\vec{r}_t$ . Integration of the overlap integral  $\langle \psi_t | \psi_{nlm} \rangle$  over angles  $\phi$  and  $\theta$  and taking into account Eqs. (10) and (11) results in

$$|\langle \psi_t | \psi_{nlm} \rangle| = \delta_{m,0} \frac{2\sqrt{\pi} Y_{l0}(0,0) e^{-\kappa R}}{j_{l+1}(\varphi_{nl})} I_l, \quad (16)$$

where

$$I_l = \int_0^1 j_l(\varphi_{nl} x) x e^{\kappa R x} dx. \quad (17)$$

For the 2.5-nm-sized NCs ( $R = 1.25$  nm),  $E_e \simeq 2.3$  eV corresponds to the energy-level  $E_{12} = 2.27$  eV and the wave function with  $n = 1$  and  $l = 2$ . Then  $\kappa R = 3.72$ , and as a result of the calculation using Eqs. (15)–(17), the probability of electron tunneling is as follows:

$$w_{e,2.5 \text{ nm}} = 4.8 \times 10^{14} \text{ s}^{-1}. \quad (18)$$

For 4- and 5.5-nm-sized NCs ( $\kappa R = 5.94$  and  $\kappa R = 8.16$ , respectively), there are two levels with energies close to  $E_e \simeq 2.3$  eV with a small difference:  $E_{15} = 2.27$  and  $E_{30} = 2.31$  eV for  $R = 2$  nm and  $E_{18} = 2.27$  and  $E_{25} = 2.33$  eV for  $R = 2.75$  nm. In this case, we have produced the calculation using Eqs. (15)–(17) for each energy level and have taken the average value as the final result. For the 4- and 5.5-nm-sized NCs this results in electron tunneling probabilities of

$$w_{e,4 \text{ nm}} = 6.3 \times 10^{13} \text{ s}^{-1}, \quad (19)$$

and

$$w_{e,5.5 \text{ nm}} = 4.9 \times 10^{13} \text{ s}^{-1}, \quad (20)$$

respectively.

In order to estimate the corresponding probabilities of exciton capture into the STE state [Eq. (7)], the overlap integral of the vibration functions corresponding to the initial and the final states in the tunneling process need to be calculated

$$\langle \Phi_n | \Phi_0 \rangle = \int_{-\infty}^{\infty} \Phi_n(Q - Q_0) \Phi_0(Q) dQ, \quad (21)$$

where the wave function of the initial state without the vibration is given by the formula,

$$\Phi_0(Q) = \left( \frac{M\omega_0}{\pi\hbar} \right)^{1/4} e^{-(M\omega_0/2\hbar)Q^2}, \quad (22)$$

and the wave function of the final state when the vibration in the adiabatic potential corresponding to the STE is excited at the vibration level  $n$  is given by the formula,

$$\Phi_n(Q) = \left( \frac{M\omega_0}{\pi\hbar} \right)^{1/4} \frac{1}{\sqrt{2^n n!}} e^{-(M\omega_0/2\hbar)(Q-Q_0)^2} H_n \left[ \sqrt{\frac{M\omega_0}{\hbar}} (Q - Q_0) \right]. \quad (23)$$

Here,  $M$  is the mass of the vibrating particle,  $\omega_0$  is the vibration frequency,  $H_n(x)$  is the Hermite polynomial of degree  $n$  of the variable  $x$ , and  $Q_0$  is the displaced equilibrium point of the adiabatic potential corresponding to the STE state (see Fig. 1).

It is convenient to calculate the overlap integral by using dimensionless coordinates  $x = \sqrt{\frac{M\omega_0}{\hbar}} Q$  and Eq. (4) for  $x_0$ . In these coordinates the overlap integral takes the form

$$\langle \Phi_n | \Phi_0 \rangle = \frac{1}{\sqrt{\pi 2^n n!}} \int_{-\infty}^{\infty} e^{-\{[(x-x_0)^2+x^2]/2\}} H_n(x-x_0) dx. \quad (24)$$

Only the two parameters  $n$  and  $x_0$  need to be known in order to calculate the overlap integral. Using Eq. (4),  $x_0 = 6.36$  and parameter  $n$  is determined by

$$n = \frac{E_{\text{EXC}} - E_{g,\text{exc}} - \varepsilon_T}{\hbar\omega_0} = \frac{E_{\text{EXC}} - E_{\text{STE}}}{\hbar\omega_0}. \quad (25)$$

For an excitation energy of  $E_{\text{exc}} = E_{\text{EXC}} = 3.6$  eV, we arrive at  $n = 13$ . Both  $x_0$  and  $n$  are independent of the size of the NC, and  $n$  depends only on  $E_{\text{exc}}$ . Using these two values together with Eq. (24), we arrive at

$$|\langle \Phi_{13} | \Phi_0 \rangle|^2 = 0.025 \quad (26)$$

for  $E_{\text{exc}} = 3.6$  eV. Using Eq. (26) in combination with the estimated probabilities of electron tunneling [Eqs. (18)–(20)], we obtain probabilities of the exciton capture into the STE state on the Si NC surface  $W_{\text{exc}}$  of  $1.2 \times 10^{13}$ ,  $1.6 \times 10^{12}$ , and  $1.2 \times 10^{12} \text{ s}^{-1}$  for 2.5-, 4-, and 5.5-nm-sized NC, respectively. These tunneling probabilities correspond to capture times of  $\sim 0.1$ ,  $\sim 0.6$ , and  $\sim 1$  ps, for NCs of 2.5, 4, and 5.5 nm in size, respectively, and are of the same order of magnitude as the experimentally obtained decay times (see Figs. 2 and 3).

The initial IA transients for different NC sizes as well as probe energies have been fitted to a single exponential function to estimate the STE capture time. The results are shown in Fig. 4 where the experimentally obtained time constants of the three samples with different NC sizes are shown for a range of probe energies. From the data, the size and probe energy dependences are clearly visible. For low probe energies, we arrive at time-constant values of  $\sim 0.4$ ,  $\sim 1.2$ , and  $\sim 1.8$  ps for the 2.5-, 4-, and 5.5-nm-sized Si NCs, respectively. For comparison, the theoretically estimated STE capture times for the three NC sizes are indicated with dashed lines. Although the theoretically estimated values are somewhat smaller (approximately a factor 2), they are of the same order of magnitude as the experimental results in the low probe energy regime and reproduce correctly the experimentally observed shortening of the capture time with decreasing NC size. Noteworthy, the experimentally obtained

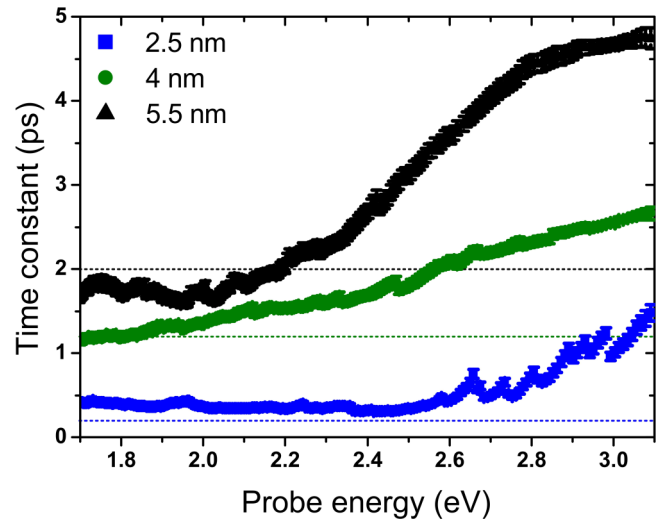


FIG. 4. Comparison of the experimentally determined initial IA decay time constant and the theoretically estimated STE capture time. The probe energy dependence of the time constant, determined by fitting the initial IA transients to a single exponential function for three samples with average NC sizes of  $d_{\text{NC}} = 2.5$  (blue), 4 (olive), and 5.5 nm (black). For comparison, the theoretically estimated STE capture times, multiplied by factor 2, for the three NC sizes are indicated with dashed lines in the same color as the corresponding experimental values.

time constant prolongs for higher probe energies, whereas the calculations predict a constant value. We suggest that for high probe energies other effects, such as optical excitation from the STE to the FE state, could also contribute to the experimentally measured carrier dynamics. The experimental data suggest that there is an onset of the increase in the time constant close to the STE threshold energy for optical excitation from the STE to the FE state  $\varepsilon_{\text{opt}}$ . When the carriers are trapped in the STE state, they are still visible for high probe energies, larger than the STE threshold, prolonging the effective lifetime for these energies. The observation of this onset evidences that the  $E_{\text{probe}}$ -dependent behavior is not due to the spectral and/or temporal stretching of the pulse, also referred to as “chirp.”

## VII. CONCLUSIONS

In conclusion, the presented transient IA measurements and theoretical modeling for  $\text{SiO}_2$ -embedded Si NCs of average NC diameters ranging from 2.5 to 5.5 nm show that the trapping process of free excitons into the STE state occurs within a few picoseconds. The trapping time of free excitons depends on the NC size, becoming longer with increasing NC size in the range of 2.5–5.5 nm. This is in good agreement with calculations within the framework of the Huang-Rhys model. The trapping times are of the same order of magnitude as the hot-carrier cooling times in this material. The STE has therefore a prominent effect on the optical properties of Si NCs. The relatively high PL quantum yield values found for Si NCs could possibly be (partially) explained by the STE state; a possible scenario could be that the STE state functions as a temporary storage of carriers, thereby preventing their nonradiative recombination through other channels.

## ACKNOWLEDGMENTS

The authors acknowledge Prof. W. J. Buma and Dr. H. Zhang (University of Amsterdam) for facilitating the IA measurements. This research was supported by the Dutch

Technology Foundation STW, which is part of the Netherlands Organisation for Scientific Research (NWO) and which is partly funded by the Ministry of Economic Affairs.

- 
- [1] L. Pavesi, L. Dal Negro, C. Mazzoleni, G. Franzò, and F. Priolo, *Nature (London)* **408**, 440 (2000).
- [2] O. Boyraz and B. Jalali, *Opt. Express* **12**, 5269 (2004).
- [3] F. Priolo, T. Gregorkiewicz, M. Galli, and T. F. Krauss, *Nat. Nanotechnol.* **9**, 19 (2014).
- [4] D. Timmerman, I. Izeddin, P. Stallinga, I. N. Yassievich, and T. Gregorkiewicz, *Nat. Photonics* **2**, 105 (2008).
- [5] E. M. L. D. de Jong, S. Saeed, W. C. Sinke, and T. Gregorkiewicz, *Sol. Energy Mater. Sol. Cells* **135**, 67 (2015).
- [6] S. Saeed, E. M. L. D. de Jong, K. Dohnalová, and T. Gregorkiewicz, *Nat. Commun.* **5**, 4665 (2014).
- [7] J.-H. Park, L. Gu, G. von Maltzahn, E. Ruoslahti, S. N. Bhatia, and M. J. Sailor, *Nature Mater.* **8**, 331 (2009).
- [8] D. Kovalev, H. Heckler, G. Polisski, and F. Koch, *Phys. Status Solidi B* **215**, 2 (1999).
- [9] M. V. Wolkin, J. Jorne, P. M. Fauchet, G. Allan, and C. Delerue, *Phys. Rev. Lett.* **82**, 197 (1999).
- [10] G. Allan, C. Delerue, and M. Lannoo, *Phys. Rev. Lett.* **76**, 2961 (1996).
- [11] W. D. A. M. de Boer, D. Timmerman, T. Gregorkiewicz, H. Zhang, W. J. Buma, A. N. Poddubny, A. A. Prokofiev, and I. N. Yassievich, *Phys. Rev. B* **85**, 161409(R) (2012).
- [12] W. D. A. M. de Boer, E. M. L. D. de Jong, D. Timmerman, T. Gregorkiewicz, H. Zhang, W. J. Buma, A. N. Poddubny, A. A. Prokofiev, and I. N. Yassievich, *Phys. Rev. B* **88**, 155304 (2013).
- [13] A. V. Gert and I. N. Yassievich, *Semiconductors* **49**, 492 (2015).
- [14] S. Takeoka, M. Fujii, and S. Hayashi, *Phys. Rev. B* **62**, 16820 (2000).
- [15] F. Trojánek, K. Neudert, P. Malý, K. Dohnalová, and I. Pelant, *J. Appl. Phys.* **99**, 116108 (2006).
- [16] A. N. Poddubny, A. A. Prokofiev, and I. N. Yassievich, *Appl. Phys. Lett.* **97**, 231116 (2010).
- [17] A. V. Gert, A. A. Prokofiev, and I. N. Yassievich, *Phys. Status Solidi A* **213**, 2879 (2016).
- [18] M. Berthe, R. Stiufiuc, B. Grandidier, D. Deresmes, C. Delerue, and D. Stiévenard, *Science* **319**, 436 (2008).
- [19] D. Goguenheim and M. Lannoo, *Phys. Rev. B* **44**, 1724 (1991).
- [20] H. A. Bethe and R. E. Peierls, *Proc. R. Soc. London, Ser. A* **148**, 146 (1935).
- [21] D. Babić, R. Tsu, and R. F. Greene, *Phys. Rev. B* **45**, 14150 (1992).
- [22] A. S. Moskalenko, J. Berakdar, A. A. Prokofiev, and I. N. Yassievich, *Phys. Rev. B* **76**, 085427 (2007).